Published in final edited form as:
Biomaterials. 2014 August ; 35(26): 7598–7609. doi:10.1016/j.biomaterials.2014.05.032.

Naturally enveloped AAV vectors for shielding neutralizing antibodies and robust gene delivery *in vivo*

Bence György[1,*], **Zachary Fitzpatrick**[1,2,*], **Matheus HW Crommentuijn**[1,3], **Dakai Mu**[1], and **Casey A. Maguire**[1,#]

[1]Department of Neurology, The Massachusetts General Hospital and Neuroscience Program, Harvard Medical School, Boston, USA [2]Louisiana State University, Baton Rouge, LA [3]Neuro-oncology Research Group, Department of Neurosurgery, Cancer Center Amsterdam, and VU University Medical Center, Amsterdam, The Netherlands

Abstract

Recently adeno-associated virus (AAV) became the first clinically approved gene therapy product in the western world. To develop AAV for future clinical application in a widespread patient base, particularly in therapies which require intravenous (i.v.) administration of vector, the virus must be able to evade pre-existing antibodies to the wild type virus. Here we demonstrate that in mice, AAV vectors associated with extracellular vesicles (EVs) can evade human anti-AAV neutralizing antibodies. We observed different antibody evasion and gene transfer abilities with populations of EVs isolated by different centrifugal forces. EV-associated AAV vector (ev-AAV) was up to 136-fold more resistant over a range of neutralizing antibody concentrations relative to standard AAV vector *in vitro*. Importantly in mice, at a concentration of passively transferred human antibodies which decreased i.v. administered standard AAV transduction of brain by 80%, transduction of ev-AAV transduction was not reduced and was 4,000-fold higher. Finally, we show that expressing a brain targeting peptide on the EV surface allowed significant enhancement of transduction compared to untargeted ev-AAV. Using ev-AAV represents an effective, clinically relevant approach to evade human neutralizing anti-AAV antibodies after systemic administration of vector.

Keywords

adeno-associated virus; extracellular vesicles; exosomes; microvesicles; gene therapy; gene delivery

[#]Corresponding author: Casey A. Maguire, cmaguire@mgh.harvard.edu, Telephone: (617) 726-5725, Fax: (617) 724-1537.
[*]These authors contributed equally to this work.

Introduction

In recent years, adeno-associated virus (AAV) vectors have shown promising results in clinical trials for the treatment of genetic diseases including, hemophilia (1), eye disease (2), lipoprotein lipase deficiency (3), and CNS disease (4). As AAV vector is comprised of the capsid of wild type (wt) virus, pre-existing immunity to wt AAV in the form of antibodies is a major concern for effective gene delivery to target tissue in patients. This is of particular importance for systemic administration of vector as the highest concentrations of anti-AAV antibodies are in blood. It has been demonstrated in mice that even low levels of neutralizing antibodies can completely abrogate liver directed gene therapy (5). This is of major concern for translation of systemic AAV-based gene therapies to a large human population, as over 50% of all people have some level of neutralizing antibodies to AAV(6).

Current strategies to evade neutralizing antibodies include genetic engineering of the AAV capsid, using empty capsids as AAV decoys, plasmapheresis, and balloon catheterization with saline flush. All of these approaches have shown promise in preclinical models, however each may have significant drawbacks precluding their widespread use clinically.

Extracellular vesicles (EVs) are endogenous nano-to-micron sized lipid particles released from cells. They carry many types of nucleic acids and proteins from the host cell in their interior as well as a multitude of receptors on their surface (7). Accumulating research suggests that EVs serve as a form of communication between cell types, and they are rapidly internalized into recipient cells (8). They can also be used for antibody evasion, as two recent studies have shown that two pathogens, hepatitis A virus (9) and hepatitis C (10), can exploit EVs to hide from patient-derived antibodies against the virus. Furthermore, they are being engineered as therapeutic delivery vehicles for nucleic acids and drugs (11, 12).

Recently we have discovered that a portion of adeno-associated virus (AAV) vector associates with microvesicles/EVs during production, (13). As recent data has shown the potential of EVs as therapeutic delivery modalities (14–16), as well as a safe profile of EVs in clinical trials (17) with more trials currently ongoing (www.clinicaltrials.gov), we postulated that EV-associated AAV (ev-AAV) may possess unique properties from standard AAV which may be beneficial for *in vivo* gene therapy applications, including antibody evasion. Here we tested whether ev-AAV could evade neutralizing antibodies against AAV in an *in vivo* model. We also explored whether decorating the surface of EVs with brain-targeting ligands would enhance specificity of gene delivery to this organ after intravenous injection of ev-AAV.

Materials and Methods

Cell Culture

Human 293T and HeLa cells were obtained from the American Type Culture Collection (Manassas, VA) and cultured in high glucose Dulbecco's modified Eagle's medium (Life Technologies, Grand Island, NY) supplemented with 10% fetal bovine serum (Sigma, St Louis, MO), 100 U/ml penicillin, and 100 μg/ml streptomycin (Life Technologies) in a humidified atmosphere supplemented with 5% CO2 at 37°C.

Targeting constructs—RVG-TM cDNA was synthesized by Aldevron (Fargo, ND). The sequence for RVG peptide is N-**YTIWMPENPRPGTPCDIFTNSRGKRASNG**-COOH.

AAV and ev-AAV production

AAV vectors and ev-AAV were produced in 293T cells as previously described (13). Briefly, a triple transfection of AAV and helper plasmids was performed using the calcium phosphate method. Standard AAV vectors were extracted from cell lysates and purified by iodixanol density gradient ultracentrifugation. Next, iodixanol was removed and vector concentrated using Amicon Ultra 100 kDa molecular weight cutoff (MWCO) centrifugal devices (Millipore, Billerica, MA) and buffer (20 mM Tris-HCl, 500 mM NaCl, pH 8.5). Next the buffer was dialysed against phosphate buffered saline (PBS) using Pierce 20 kDa MWCO Slide-A-Lyzer MINI Dialysis Device (Pierce, City, State) and finally filtered through a 0.22 um Millex-GV Filter Unit (Millipore).

For ev-AAV, media was changed to EV-free 2% FBS the day after transfection. At 48 and 72 h post transfection, media was harvested. Cell debris and apoptotic bodies were removed by sequential, 10 min 300 × g and 2000 × g centrifugations, respectively. The supernatant containing vexosomes was then centrifuged at 20,000 × g for 2 h. The media was aspirated and the EV/ev-AAV pellet was resuspended in PBS. For the 100k × g ev-AAV, we performed the same low speed 300 × g and 2000 × g steps followed by the 20,000 × g pelleting. All of these pellets were discarded and the remaining media was centrifuged at 100,000 × g for 1 hour using a Type 70 Ti rotor in a Optima™ L-90K ultracentrifuge (both Beckman Coulter, Inc., Indianapolis IN). The resulting pellet was resuspended in PBS. Both ev-AAV and standard AAV preparations were stored at −80°C until use. For bioluminescence imaging we used a single-stranded AAV construct encoding firefly luciferase (FLuc) driven by the CBA promoter (18). For immunofluorescence analysis of transduced cell types we used a self-complementary AAV construct encoding eGFP driven by the CBA promoter. To titer AAV and ev-AAV preparations, a quantitative TaqMan PCR that detects AAV genomes (poly(A) region of the transgene cassette) was performed as previously described (13).

Mice

All animal experiments were approved by the Massachusetts General Hospital Subcommittee on Research Animal Care following guidelines set forth by the National Institutes of Health Guide for the Care and Use of Laboratory Animals. Female nude mice aged 6–8 weeks were purchased from the National Cancer Institute. Female Balb/c mice aged 6–8 weeks were purchased from Jackson Laboratory (Bar Harbor, ME). For tail vein injections of AAV vectors and vexosomes, mice were placed into a restrainer, (Braintree Scientific, Inc., Braintree, MA). Next the tail was warmed in 40°C water for 30 seconds, before wiping the tail with 70% isopropyl alcohol pads. A 100–300 μl volume of vector (in PBS) was slowly injected into a lateral tail vein, before gently finger clamping the injection site until bleeding stopped.

Bioluminescence imaging of firefly luciferase (FLuc) expression

Imaging was performed using an IVIS® Spectrum optical imaging system fitted with an XGI-8 Gas Anesthesia System (Caliper Life Sciences, Hopkinton, MA). Mice were anesthetized and then injected intraperitoneally with 4.5 mg of $_D$-luciferin resuspended in 150 μl of PBS. Five minutes post-substrate injection, mice were imaged for luciferase expression using auto-acquisition. Bioluminescent images were acquired using the auto-exposure function. Data analysis for signal intensities and image comparisons were performed using Living Image® software (v. 4.3.1, Caliper Life Sciences). To calculate total flux in photons/sec for each animal, regions of interest (ROIs) were carefully drawn around each area of signal.

Antibody evasion experiments—*In vitro* neutralization assays were performed with 10-donor pooled normal human serum (Innovative Research, Novi, MI) or Gammagard S/D purified intravenous immunoglobulin (IVIg), (Baxter, Deerfield, IL, kindly provided by Dr. Luk H. Vandenberghe, Harvard Medical School). HeLa cells were seeded at 50,000 cells per well in a 96 well plate the day before the assay. Next, a dose of 5×10^8 g.c. of AAV9-Fluc or ev-AAV9-Fluc was mixed with serial dilutions of human serum or IVIg in in FBS-free media to yield the indicated concentrations in the figures. AAV with no human serum served as control. These were incubated for 1 h at 37°C before adding to cells for 1.5 h at 37°C. After washing cells one time, and replacing with complete medium, cells were incubated for 48 h before performing a luciferase assay using Bright-Glo™ Luciferase reagent (Promega, Madison, WI). Luciferase values for each sample, expressed in relative light units (RLUs) were plotted as a percentage of the AAV transduction sample without serum (which was set to 100%).

In vivo neutralization assays

Mice were injected intraperitoneally (i.p.) with the indicated amount of IVIg in PBS (total volume 200 μl). Twenty four hours later mice were injected i.v. via the tail vein with 10^{10} g.c. of either AAV9-FLuc or ev-AAV9-FLuc in a volume of 200 μl. Mice were imaged at the indicated time points for FLuc-associated bioluminescence.

Ex-vivo organ luciferase assay

32 days post-vector injection, mice were sacrificed and organs were harvested for analysis of FLuc levels. Tissues were quickly removed from the animals, and immediately frozen on liquid nitrogen and stored at −80 °C. For FLuc assay, 50 mg of each tissue was placed in 2 ml tubes containing 1.4 mm ceramic beads (Mo Bio Laboratories, Inc., Carlsbad CA) and 500 μL of Mammalian Protein Extraction Reagent (M-PER; Pierce Biotechnology, IL, USA). Tissues were homogenized in a BeadBug microtube homogenizer (Benchmark Scientific, Edison, NJ). Next, tubes were centrifuged for 5 minutes at 300 × g and 20 μL of tissue homogenate was transferred to 96-well white bottom plate and analyzed using 100 μL of Bright-Glo™ FLuc substrate reagent (Promega, WI, USA) and a plate luminometer (Dynex Technologies, VA, USA). A Bradford assay (Bio-Rad, Hercules, CA) was performed to normalize each FLuc value to the total amount of protein in the sample.

Iodixanol isopycnic density gradient

To characterize AAV in the 20k × g depleted media, an iodixanol step gradient was made similar to (9) with the exception that we added a 60% layer at the bottom. The media sample was concentrated to from 20 to 2 ml using Amicon Ultra 100 kDa molecular weight cutoff (MWCO) centrifugal devices and loaded on the top of the gradient. The gradient was centrifuged at 125,755 × g for 16 h in an SW32 Ti rotor (Beckman Coulter). Two ml fractions were collected for AAV qPCR.

Removing EVs from 293T conditioned media

Media was centrifuged at 300 × g for 5 min and then 2,000 × g for 10 min, followed by a 100,000 × g centrifugation in a Type 70 Ti rotor (Beckman Coulter). The supernatant was transferred to a new tube and then filtered sequentially through 0.8 μm, 0.22 μm and 0.05 μm filters to remove any remaining EVs.

Histology and GFP expression

At two weeks post-injection, mice were given an overdose of anesthesia and transcardially perfused with PBS and 4% PFA. The brain was removed. The brain was post-fixed in 4% formaldehyde in PBS for 2 h and cryoprotected for three days in 30% sucrose and then frozen in a dry ice/2-methylbutane bath for immunohistological analysis of tissue sections. Brains were cut on the coronal plane in 40 μm sections using a sledging freezing microtome. Immunofluorescence was performed in free-floating sections with a primary antibody for GFP (rabbit anti-GFP, GFP Abfinity, 1:400, Life Technologies). Briefly, the sections were permeabilized in PBS with Triton-X 0.5% for 2 h, blocked in 5% normal goat serum for 1 h, and incubated with the primary antibody 60 h at 4°C. The sections were thoroughly washed in PBS, incubated with 1:1000 goat anti-rabbit Fab2 Alex Fluor 488-conjugated antibody (Cell Signaling, Danvers, MA) for 1 h at room temperature, washed again in PBS, and coverslipped with fluorescent mounting media (Dako). Neurons, endothelial cells and astrocytes were readily distinguished from each other using morphological criteria.

In vitro targeting of RVG-TM-ev-AAV9

SH-SY5Y cells were cultured in EMEM/F12 medium with 10% FBS and 1% penicillin/streptomycin. Cells were seeded at 50,000 cells/well in 96 well plates 24 hours before transduction. 5×10^7 g.c. of standard ev-AAV9-FLuc or RVG-ev-AAV9-FLuc were preincubated either with heparin (50 μg/mL), or with heparin and RVG (100 μM) for 30 minutes at RT. Cells were transduced for 1 hour at 37°C. FLuc assay was performed 48 hours post-transduction using Bright-Glo™ FLuc substrate reagent (Promega, WI, USA) and a plate luminometer (Dynex Technologies, VA, USA).

Calculations—Brain to peripheral organ transduction ratio (Figure 4b). To calculate the targeting efficiency of each vector we compared the luciferase activity in the brain to the sum of the activity in the peripheral organs analyzed (liver, lung, heart, muscle, spleen, kidney). We used the following formula:

$$\text{Brain:peripheral transduction ratio} = \frac{(\text{Avg. Brain RLU/mg})}{(\text{Avg. Liver RLU/mg}) + (\text{Avg. Lung RLU/mg}) + (\text{Avg. Spleen RLU/mg}) + \ldots\ldots}$$

Statistics—Statistical analyses were performed using GraphPad Prism software (version 5.01). For comparisons of means between two groups an unpaired t-test was used. For comparison of three or more groups, a one-way ANOVA was used followed by a Tukey post test to compared two means. Statistical significance was determined at a value below 0.05.

Results

ev-AAV resists anti-AAV antibodies from pooled human serum and purified immunoglobulin

We produced and isolated standard AAV9 encoding firefly luciferase (AAV9-FLuc) and ev-AAV9-FLuc from the cell lysates and media, respectively, of the same preparation of vector (Supplementary Fig. 1) as previously described (13). AAV9-FLuc or ev-AAV9-FLuc were mixed with dilutions of complement-inactivated human sera from 10 donors and incubated for 1 h at 37°C before adding the mixture to cells for 1 h at 37°C. Media was replaced on cells and then they were incubated for 48 h before harvesting for a luciferase assay. Luciferase activity at each dilution was normalized to the transduction of the vector in the absence of serum. Strikingly, we observed that ev-AAV9 was 3 to 23-fold more resistant to neutralization than AAV9 at the 1:20–1:80 dilutions, respectively (Fig. 1A). The resistance was not due to a non-specific effect of EVs adsorbing antibody, as standard AAV9 mixed with free EVs from untransfected cells (same amount of EVs as for ev-AAV preparation) did not achieve significantly higher protection relative to standard AAV9 (Fig. 1B). Next we incubated AAV9-FLuc or ev-AAV9-FLuc with dilutions of purified immunoglobulin (intravenous immunoglobulin, IVIg, from multiple donors' plasma). Similar to the human serum data in Fig. 1a we observed up to a 25-fold increased resistance to antibody neutralization with ev-AAV9 compared to standard AAV9 (Fig. 1C). We also observed that ev-AAV1 and ev-AAV2 were more resistant to serum compared to their standard serotypes (Supplementary Fig. 2). To ensure that the increased resistance to neutralizing antibodies was not due to a shielding ability of excess empty capsids in the ev-AAV preparation obtained from media (compared to the standard AAV purified by iodixanol density gradient) we treated media samples of ev-AAV2 using a pulldown that consists of a monoclonal antibody which recognizes intact capsids bound to magnetic beads. We first confirmed that the pulldown efficiently removed free AAV2 by incubating standard AAV2 with the beads, finding that it removed ~80% of free vector as assessed by qPCR for vector genomes (Supplementary Fig. 3A). Next, we mixed ev-AAV2-FLuc with the anti-AAV2/magnetic bead conjugate or an isotype control/magnetic bead conjugate which does not pulldown AAV2 capsids. The AAV remaining in media after pulldown with either antibody was quantitated by qPCR and equal g.c. were mixed with dilutions of pooled human serum. If a molar excess of free AAV2 capsids in the ev-AAV preparation were blocking neutralizing of the EV-associated vector than it would be expected that the sample treated with anti-AAV2 pulldown would be more susceptible to neutralization. However, this was not the

case as we saw nearly identical neutralization assay profiles for the control and anti-AAV2 antibody pulldowns (Supplementary Fig. 3B). Free AAV2 was used as control and showed greater susceptibility to neutralization than the ev-AAV preparations, as expected (Supplementary Fig. 3B).

We then analyzed whether ev-AAV9 could transduce cells *in vivo* in the presence of anti-AAV immunoglobulin as *in vivo* neutralization assays are thought to more accurately predict the human situation (5). We first determined the amount of IVIg that would neutralize standard AAV9 in mice. Nude mice were injected i.p. with a range of IVIg amounts and 24 h later, injected i.v. with 10^{10} g.c. of AAV9-FLuc. Imaging mice for luciferase expression four days later determined that 0.1 mg and 1.0 mg reduced transduction of AAV9-FLuc by 83% and 98%, respectively, compared to naïve mice (Supplementary Fig. 4). We chose an equidistant dose of 0.5 mg IVIg to compare AAV and ev-AAV resistance to antibody neutralization. Mice were injected i.p. with 0.5 mg IVIg or PBS and 24 h later, i.v. with 10^{10} g.c. of AAV9-FLuc or ev-AAV9-FLuc. Seven days later imaging of liver region revealed that AAV9-FLuc had residual transduction of 1.5% in the presence of IVIg while it was 8.38% for ev-AAV9-FLuc ($p=.099$, Fig. 2 A, B). We also measured the light emission from the head region of all injected mice. We found AAV9-FLuc had residual transduction of 2.6% while ev-AAV9-FLuc was 18.9% ($p=0.0085$, Fig. 2 C, D). These data indicate that ev-AAV9 is more resistant to IVIg *in vivo* relative to standard AAV.

We routinely harvest ev-AAV from the EV pellet obtained from centrifuging at 20,000 × g. This spin force vs. a higher speed was chosen from our prior research (13) as it minimized co-pelleting of any free-AAV in media. We wondered if the small vesicle fraction of ev-AAV (obtained by ultracentrifuging media at 100,000 × g) would display antibody evasion characteristics. From the same batch of AAV9-FLuc producer cells, we harvested standard AAV from cell lysates and then from media in the 20,000 × g (20k × g) and subsequently the 100,000 × g (100k × g) ev-AAV9-FLuc pools. An *in vitro* neutralization assay using IVIg was performed on HeLa cells. Remarkably, the 100k × g ev-AAV pool was much more resistant to neutralization compared to both the 20k × g ev-AAV pool and standard AAV9-FLuc. (Fig. 3A). For example at the 2 mg/ml concentration of IVIg, the 100k × g ev-AAV retained 57% of its transduction capacity in the absence of antibodies, while the values were just 7% and 0.42% for 20k × g ev-AAV and AAV, respectively (Fig. 3A). We next performed an *in vivo* neutralization assay comparing standard AAV to the 100k ev-AAV using the same conditions as in Fig. 2. Imaging at two weeks post injection revealed a 78.5% reduction for standard AAV9-Fluc in the presence of IVIg (Fig. 3B–D). Notably, transduction was not decreased by IVIg (118% of control) for 100k × g ev-AAV9-FLuc (Fig. 3B–D). Importantly, ev-AAV9 had 722-fold and 4,000-fold higher transduction than standard AAV with PBS and IVIg pretreatment, respectively (Fig. 3C). To characterize the AAV in the 20k × g-depleted media fraction used to isolate 100k × g ev-AAV, we placed this media on an 8–60% iodixanol isopycnic gradient. We compared this to cell lysate-purified AAV run on a similar gradient. Expectedly, for standard AAV, 96% of vector genomes loaded onto the gradient migrated in the 40–60% area at the bottom of the gradient (Fig. 4A). In contrast a distinct fraction of AAV in the 20k × g depleted media (~10%) ran in the 14–20% (fractions #5–9) concentration of iodixanol which is suggestive of a less-

dense, vesicle-associated vector (Fig. 4A, **gray arrow**). Differences were also noted in the 40–60% layers for the two samples. For example only 1% of AAV in media ran in fraction #15 while there was 20% of total genomes in the same fraction for the standard AAV sample (Fig. 4A, **blue arrows**). Also in fraction #17 there was only 14% of standard AAV genomes while there was 36% for AAV in media (Fig. 4A). To confirm that the fraction in the 14–20% layers was vesicle associated, treatment of the media with the detergent Igepal CA-360 as done by (9) greatly shifted the peak to a lower density, suggesting lysis of EVs (Fig. 4B). Interestingly, detergent treatment decreased the % AAV genomes in the #17 fraction and increased it in fraction #15, suggesting separation of some type of complex of AAV in the media (Fig. 4B, 4C). Two ascertain whether the different fractions were resistant to IVIG, we subjected the putative vesicle fraction (#6–7) and free AAV fraction (#16–17) to control PBS or IVIG. As expected the vesicle fraction was completely resistant to IVIG, while fractions #16,17 was sensitive (free AAV was used as control in the assay, Fig. 4D). Since the vesicle fraction was only 10% of the AAV genomes on the gradient and in our *in vitro* and *in vivo* neutralization assays (Fig. 3) the 100k × g ev-AAV are extremely resistant to IVIG, we wondered if the 100k × g centrifugation process caused an association of “free AAV” in the media with the vesicle fraction of endogenous ev-AAV. To test this we compared the traditional 100k × g ev-AAV isolated from 293T producer cell media, standard AAV mixed with conditioned 293T media (20k × g vesicle-depleted) and pelleted by ultracentrifugation at 100k × g, or with standard AAV mixed with conditioned 293T media (and pelleted by 100k × g ultracentrifugation) which had all vesicles removed via an ultracentrifugation and tiered filtration process. Interestingly, simply mixing standard AAV with conditioned media and ultracentrifuging the sample led to IVIG resistance comparable to the 100k × g ev-AAV (Fig. 4E). Removing vesicles from the conditioned media, returned the IVIG sensitivity to AAV (Fig. 4E). Supporting these findings, we found that all fractions of 100k × g ev-AAV run on a sucrose gradient were resistant to IVIG (Supplementary Fig. 5 A, B) suggesting a tight association of any free AAV with the EV fraction after centrifugation. To understand how well free AAV9 pelleted in the presence of EVs under 20k × g and 100k × g centrifugal forces, we mixed free AAV9 with non-transfected 293T conditioned media (containing EVs) and by qPCR, titered an aliquot of media before spinning, and then titered the 20k × g and 100k × g fractions. We did the same experiment except with ev-AAV9 containing media from transfected 293T (Table I). From this data we were able to determine the percentage of AAV in each fraction. As expected from previous research (13), we found that 20k × g centrifugation did not pellet free AAV mixed with EVs (less than 0.1%), while the 20k × g ev-AAV9 fraction had over 1 log higher g.c. However the 100 k × g centrifugation pelleted 38% of total AAV in media in the mixed EV + AAV sample and 40% in the ev-AAV9 sample. From this data, we concluded the 20k × g ev-AAV9 fraction represents a bona-fide EV associated fraction not caused by the centrifugation technique. The 100k × g fraction appears to be an association of free AAV with ev-AAV, partially attributed to the centrifugation procedure.

To gain insight into the mechanism of enhanced transduction in culture by ev-AAV9, we performed experiments using agents which EVs are specifically sensitive to. We have previously shown that uptake of 293T–derived EVs into recipient cells is blocked by heparin (13) (19). Another group showed that heparan sulfate proteoglycans on recipient cells are

required for uptake of tumor cell-derived EVs(20). Based on these data, we reasoned that 20k × g ev-AAV9 mediated transduction would be heparin-sensitive while standard AAV9 would not, as its receptor is galactose residues (21). As predicted, transduction with AAV9-FLuc was not inhibited with heparin co-incubation while the same condition blocked 20 k × g ev-AAV9-FLuc transduction by 84% ($p<0.001$) (Fig. 5A). As the EV membrane is sensitive to low concentrations of detergent (22), we found that 20k × g ev-AAV9-Fluc transduction was significantly inhibited (75%) with Triton-X-100, while it had no effect on standard AAV9-Fluc ($p<0.05$)(Fig. 5B). Next we compared the sensitivity of the 100k × g ev-AAV9 fraction to heparin and Triton block. We found that the 100k × g fraction was not sensitive to heparin blockade at 50 μg/ml (data not shown) and increasing to 100 μg/ml slightly blocked both AAV9 and 100k × g ev-AAV9 (Fig. 5C). Transduction of cells by 100 k × g ev-AAV9 fraction was slightly sensitive (33% decrease) to Triton pretreatment (Fig. 5D) but this did not reach statistical significance. However, treatment of either 20k × g or 100k × g ev-AAV9 samples with Triton, significantly enhanced sensitivity to IVIG, showing EV-mediated protection from anti-AAV antibodies (Fig. 5E).

During the course of *in vitro* neutralization experiments, we observed that the 20k × g vexosomes transduced cells much more efficiently than standard AAV9-FLuc. We next tested transduction of 20k × g ev-AAV9-FLuc compared to standard AAV on three different cell types (primary murine neurons, SH-SY5Y cells, and melanocytes). In each case, ev-AAV9 vastly and significantly outperformed standard AAV at transduction efficiency (Fig. 6A–C). Remarkably, the 100k × g ev-AAV9 pool transduced HeLa cells 18 and 263-fold higher than the 20k × g ev-AAV pool and standard AAV, respectively, (Fig. 6D).

As our previous experiments were performed in immunocompromised nude mice with no functional T cell-mediated immunity, we next asked whether transduction with ev-AAV in immunocompetent Balb/c mice would result in stable gene expression. Mice were injected i.v. with either standard AAV2-FLuc or ev-AAV2-FLuc and imaged at day 7 and day 28 post injection. We found a rapid onset of FLuc expression with ev-AAV2 compared to AAV2 (30-fold difference at day 7, Supplementary Fig. 6). Interestingly, ev-AAV2 and AAV2 had almost identical levels of Fluc expression by day 28, 1.8×10^7 photons/sec vs. 1.4×10^7 photons/sec, respectively (Supplementary Fig. 6). Between day 7 and 28 for ev-AAV2 there was a slight 40% reduction in Fluc expression, which is not indicative of a massive T cell response against the vector/transgene product.

Brain targeting with RVG-tagged ev-AAV after i.v. injection

Having shown superiority of ev-AAV over standard AAV in antibody evasion, we next tested whether we could enhance the gene delivery capacity of vexosomes for brain. We prepared ev-AAV9-FLuc as well as ev-AAV9-FLuc from cells that were co-transfected with a mammalian expression vector encoding for platelet-derived growth factor transmembrane (TM) domain fused with rabies virus glycoprotein (RVG) peptide for targeting of ev-AAV to the brain (RVG-ev-AAV9-FLuc, Supplementary Fig. 1, 7,8) (23). The TM construct has previously been used to express ligands on the surface of cells and EVs (13, 24) and a general guideline and schematic is shown in Supplementary Fig. 7. Per our original studies (13), we utilized the 20,000k × g ev-AAV fraction for the targeting experiments. We

detected the RVG-TM mRNA in transfected cells using a reverse-transcriptase (RT) PCR with primers specific for the entire cDNA (Supplementary Fig. 8B). The RVG peptide binds to alpha-7 nicotinic acetylcholine receptor (AchR), which is expressed on SH-SY5Y cells (25) and Supplementary Fig. 9B). Based on our results in Figure 5 showing that heparin greatly reduced ev-AAV9-mediated transduction, we reasoned that RVG-ev-AAV9 would be less sensitive to heparin blockade than untargeted ev-AAV9 as it could use an alternative receptor. SH-SY5Y cells were transduced with untargeted ev-AAV9-FLuc or RVG-ev-AAV9-FLuc in the presence or absence of 50 μg/ml of heparin. As expected, transduction with untargeted ev-AAV9 was inhibited significantly more ($p<0.05$, 90% inhibition) with heparin compared to RVG-targeted ev-AAV9 (80% inhibition, Supplementary Fig. 9A, B). To further show RVG binding specificity to AchR, we also did a heparin/RVG peptide co-block at the time of transduction with either vector. As expected the addition of excess soluble RVG peptide to heparin mix significantly ($p<0.05$) decreased transduction of RVG-ev-AAV9-FLuc and not untargeted ev-AAV (Supplementary Fig. 9B).

To ascertain the brain targeting potential of RVG targeted ev-AAV, female nude mice (n=4/group) were injected intravenously (i.v.) via the tail vein with 6.5×10^{10} g.c. with ev-AAV9-FLuc, or RVG-ev-AAV9-FLuc and at various time points mice injected with $_{D}$-luciferin substrate and imaged for light emission corresponding to FLuc expression. We first analyzed luminescent images of the head region for ev-AAV9-FLuc and RVG-ev-AAV9-FLuc injected mice to detect signal in the brain region. Remarkably distinct signal emanating from the brain could be seen in RVG-ev-AAV9-FLuc mice but not ev-AAV9-FLuc mice (Fig. 7A). We also noted a higher luminescent signal in liver for RVG-ev-AAV9 injected mice compared to ev-AAV9 injected mice (Supplementary Fig. 10). To accurately measure FLuc levels throughout the brain in all groups of mice, we sacrificed animals at day 32 post injection and removed major organs including the brain. The brain was cryosectioned coronally in 1 mm sections (Fig. 7B, **photo**) and tissue homogenized and an FLuc assay performed in a luminometer with values normalized to protein content (Fig. 7B, **graph**). RVG-ev-AAV9-FLuc displayed 3–4-fold higher FLuc activity in all sections than ev-AAV9-FLuc (Fig. 7B). The average RLU/mg for each group was calculated from sections in the striatum revealing that RVG-ev-AAV9-FLuc was significantly higher than ev-AAV9-FLuc (4.8-fold, $p<0.05$) (Fig. 7C). Next we quantitated the luciferase activity in peripheral organs (liver, lung, spleen, heart, muscle, and kidney). In liver homogenates, luciferase levels were significantly lower ($p<0.05$) for ev-AAV9 (11-fold) than RVG-ev-AAV9-FLuc (Fig. 8A). Transduction of the heart was significantly lower (13-fold, $p<0.05$) for RVG-ev-AAV9 compared to ev-AAV9 (Fig. 8A). To gain insight into the brain targeting efficiency of the two vectors, we calculated the brain to peripheral transduction ratio (see Online Methods for formula). RVG-ev-AAV9-FLuc significantly ($p<0.05$) outperformed ev-AAV9 (4.7-fold) in this measure of targeting efficiency (Fig. 8B).

To analyze the cells of the brain transduced by RVG-ev-AAV9, we produced RVG-ev-AAV9 vexosomes encoding GFP. Mice were injected i.v. with 2.0×10^{10} g.c. of vector and two weeks later sacrificed, perfused, and brains fixed and cryosectioned. Sections were immunostained to detect GFP. We detected transduced neurons, astrocytes, and endothelial cells (Fig. 8C i–iv) all of which are targets of standard AAV9 after i.v. injection.

Discussion

Preclinical and clinical data has revealed that pre-existing neutralizing antibodies to wild type AAV, even at relatively low titers, can severely limit efficient gene transfer and subsequent expression by AAV vectors (5, 26–29). Seroprevalence calculations in the literature may under represent the clinical impact of low levels of antibodies, both neutralizing and non-neutralizing. Many studies start their serum dilutions at 1:20 and do not include a large percentage of people with these low anti-AAV antibody levels. It has been shown that anti-AAV antibody titers as low as 1:3.3 can completely block transduction *in vivo*, while having a negligible impact on neutralization of AAV in cultured cells (5). Since the majority of people have titers of at least 1:1, for AAV-based gene therapy to be useful for a large patient population, it is imperative that next-generation AAV vectors evade neutralizing antibodies, or there are effective procedures to remove these antibodies from circulation.

It is becoming increasingly clear that classically defined non-enveloped viruses may associate with cell membranes upon exit from the cell surface and may retain this association for at least some time in the extracellular environment (9, 10, 30, 31). This process differs from conventional cell lysis for host cell escape in the case of a non-enveloped virus. Besides pointing to important steps in the viruses' life cycle which may provide information on pathogenesis, extracellular vesicle-associated virus provides a unique strategy for manipulating current gene therapy vectors, including AAV (13). We found that ev-AAV9 could efficiently evade neutralizing antibodies when compared to standard vector. This was true for pooled human serum as well as purified pooled human IgG (Figs. 1–3).We first performed *in vitro* neutralization assays, which were confirmed with the more robust *in vivo* passive antibody transfer neutralization assay. Interestingly we observed major differences in both the transduction properties, as well as the level of antibody evasion by isolating ev-AAV9 from two different differential centrifugation speeds. We found that ev-AAV9 isolated from a 20,000 × g centrifugation had its cell culture tropism dependent on the vesicle (heparin and triton sensitive). eAAV9-FLuc was up to 42-fold more efficient at transducing a variety of cells than standard AAV9-FLuc (Fig. 6). AAV9 is known to be relatively inefficient at transduction in culture (21) and often a more efficient serotype (e.g. AAV2) has to be used in culture experiments to test the effect of the transgene of interest before moving forward with *in vivo* experiments with AAV9. ev-AAV9 is a valuable tool as it allows one to use the same serotype *in vitro* and *in vivo*. On the other hand, ev-AAV9 isolated from a 100,000 × g centrifugation, was heparin-insensitive in culture. The latter ev-AAV9 fraction was much more efficient at transduction in cell culture than the 20,000 × g fraction and much more resistant to antibodies. Amazingly, the 100k × g ev-AAV9 fraction mediated 722-fold higher levels of levels of FLuc activity in the head of mice after i.v. injected relative to standard AAV. This transduction was not affected by a dose of IVIg that reduced standard AAV by 80%, increasing the transduction differential to 4,000-fold. We showed in various assays that the resistance to anti-AAV antibodies to the 100k × g ev-AAV sample was vesicle mediated (Fig.4A–E). Interesting, we were able to create an IVIg resistant AAV by mixing AAV and 293T media containing EVs and centrifuging at 100k × g (Fig. 4E). In the future it may be possible to mix purified EVs

derived from other cell types (with various properties such as immunomodulation) to create antibody-evading AAVs. Although it has recently been suggested that the majority of AAV in producer cell media is full and has a genome (32), we wanted to rule out the possibility that free empty capsids in the 100k × g ev-AAV9 fraction were responsible for antibody evasion. We purified the 100k × g ev-AAV9 fraction on a sucrose gradient which we have previously used to separate free AAV from ev-AAV (13). We isolated fractions from the gradient, titered them for genomes by qPCR and then separately tested them in an IVIg neutralization assay (Supplementary Fig. 5A). All fractions were resistant to neutralization, indicating free empty AAV was not likely responsible for antibody evasion in this fraction (Supplementary Fig. 5B). Furthermore our data showing that Triton treatment of the 20k × g and 100k × g ev-AAV samples increased sensitivity to IVIg neutralization supports the notion that resistance is vesicle-mediated (Fig. 5E).

Other methods to overcome antibody neutralization include pre-treating naïve animals with anti-CD4 antibodies before vector administration (33), empty capsid decoys which absorb neutralizing antibodies (34), plasmapheresis to remove antibodies from blood (35), balloon catheters and saline flush (36), and engineered capsids which antibodies do not bind efficiently (37). All of these methods, while promising and useful in certain situations, have limitations. For example, strategies such as antibody and pharmacological-mediated immune modulation, plasmapheresis, and balloon catheters are not applicable to countries/regions with inadequate medical technology/infrastructure. The strategy of using excess empty capsids may induce CTL activity against transduced cells as well as compete with transgene-containing vector for binding sites in certain organs/structures with limited receptor densities. Finally engineered capsids, while able to avoid neutralizing antibodies, are often inferior to the parental vector for transduction of the tissue of interest.

One benefit of using enveloped, compartmentalized AAV for evasion of antibodies is that it requires no supplemental medical interventions in addition to the unmodified vector itself. The vector harvested from media is in a ready-to-use final formulation. Furthermore, this strategy should be applicable to any serotype.

The second significant finding of our study is that modifying the surface of EV with targeting ligands is an economical, fast, and easy approach to altering AAV transduction *in vivo*. We chose to use the AAV9 serotype for our studies as it is able to cross the BBB and efficiently transduce cells in the brain (38), our target organ. This multistep feature, most likely includes pre and post cellular entry steps and combined with the shielding properties of EVs, would potentially yield a powerful gene delivery system. We were able to show brain-selective targeting compared to untargeted ev-AAV9 after intravenous delivery (Figs. 7, 8). Typical approaches to this goal involve genetically modifying the capsid (39) which is a tedious process, often taking several months to generate vectors of interest. An even more complex approach uses virus libraries and *in vivo* selections (40) (41), which requires a great deal of expertise and experience to perform, and even then success is achieved after a trial and error approach. Using extracellular vesicle ligand display, the targeting ligand-TM construct (usually less than 400 b.p.) is synthesized by a variety of companies for low cost. The process from ordering the ligand-TM construct to ev-AAV9 production is approximately 3 weeks. Production of ev-AAV9 and harvest from media is simple.

In addition to increased brain transduction, we observed RVG-ev-AAV9 to have enhanced transduction of the liver compared to ev-AAV9. The RVG peptide binds to the nicotinic acetylcholine receptor (AchR) which is expressed on neurons. AchR is also expressed on macrophages (42) and it is possible that RVG-ev-AAV9 is transducing liver macrophage. In the future, it may be possible to avoid liver macrophage with this targeting approach by injecting via the intracarotid artery route so that the first pass of vector through the circulatory system reaches the brain before liver.

Conclusions

We have shown that extracellular vesicles (EVs) can be utilized to overcome neutralizing antibodies to a gene therapy vector *in vivo*. We also observed that EV-associated AAV9 can outperform standard AAV9 at transduction efficiency in culture and *in vivo*. Finally, we show that expression of engineered transmembrane ligands on the surface of EVs can allow enhanced AAV-encoded gene delivery to target tissue. These properties bestowed by EVs on AAV vectors may have direct clinical relevance for antibody evasion and may be applied to other vector systems.

Supplementary Material

Refer to Web version on PubMed Central for supplementary material.

Acknowledgments

This work was supported by a grant from NIH/NINDS R21 NS081374-01 (CM). BG was supported by NIH grant R01DC02281 to David P. Corey. CM has a financial interest in Exosome Diagnostics, Inc. CM's interests were reviewed and are managed by the Massachusetts General Hospital and Partners HealthCare in accordance with their conflict of interest policies. CM has filed patent applications related to the ev-AAV (vexosome) technology. We would like to acknowledge the Neuroscience Center Nucleic Acid Quantitation Core and Image Analysis Core (supported by NINDS P30NS045776). We thank Bakhos A. Tannous for technical advice regarding the RVG-TM construct.

REFERENCES

1. Nathwani AC, Tuddenham EG, Rangarajan S, Rosales C, McIntosh J, Linch DC, et al. Adenovirus-associated virus vector-mediated gene transfer in hemophilia B. N Engl J Med. 2011; 365(25): 2357–2365. [PubMed: 22149959]
2. Maguire AM, High KA, Auricchio A, Wright JF, Pierce EA, Testa F, et al. Age-dependent effects of RPE65 gene therapy for Leber's congenital amaurosis: a phase 1 dose-escalation trial. Lancet. 2009; 374(9701):1597–1605. [PubMed: 19854499]
3. Haddley K. Alipogene tiparvovec for the treatment of lipoprotein lipase deficiency. Drugs Today (Barc). 2013; 49(3):161–170. [PubMed: 23527320]
4. Muramatsu S, Fujimoto K, Kato S, Mizukami H, Asari S, Ikeguchi K, et al. A phase I study of aromatic L-amino acid decarboxylase gene therapy for Parkinson's disease. Mol Ther. 2010; 18(9): 1731–1735. [PubMed: 20606642]
5. Scallan CD, Jiang H, Liu T, Patarroyo-White S, Sommer JM, Zhou S, et al. Human immunoglobulin inhibits liver transduction by AAV vectors at low AAV2 neutralizing titers in SCID mice. Blood. 2006; 107(5):1810–1817. [PubMed: 16249376]
6. Louis, Jeune V.; Joergensen, JA.; Hajjar, RJ.; Weber, T. Pre-existing anti-adeno-associated virus antibodies as a challenge in AAV gene therapy. Hum Gene Ther Methods. 2013; 24(2):59–67. [PubMed: 23442094]

7. Mathivanan S, Fahner CJ, Reid GE, Simpson RJ. ExoCarta 2012: database of exosomal proteins, RNA and lipids. Nucleic Acids Res. 2012; 40:D1241–D1244. (Database issue). [PubMed: 21989406]
8. S ELA, Mager I, Breakefield XO, Wood MJ. Extracellular vesicles: biology and emerging therapeutic opportunities. Nat Rev Drug Discov. 2013; 12(5):347–357. [PubMed: 23584393]
9. Feng Z, Hensley L, McKnight KL, Hu F, Madden V, Ping L, et al. A pathogenic picornavirus acquires an envelope by hijacking cellular membranes. Nature. 2013; 496(7445):367–371. [PubMed: 23542590]
10. Ramakrishnaiah V, Thumann C, Fofana I, Habersetzer F, Pan Q, de Ruiter PE, et al. Exosome-mediated transmission of hepatitis C virus between human hepatoma Huh7.5 cells. Proc Natl Acad Sci U S A. 2013; 110(32):13109–13113. [PubMed: 23878230]
11. Tian Y, Li S, Song J, Ji T, Zhu M, Anderson GJ, et al. A doxorubicin delivery platform using engineered natural membrane vesicle exosomes for targeted tumor therapy. Biomaterials. 2014; 35(7):2383–2390. [PubMed: 24345736]
12. Zhang Y, Li L, Yu J, Zhu D, Zhang Y, Li X, et al. Microvesicle-mediated delivery of transforming growth factor beta1 siRNA for the suppression of tumor growth in mice. Biomaterials. 2014; 35(14):4390–4400. [PubMed: 24565517]
13. Maguire CA, Balaj L, Sivaraman S, Crommentuijn MH, Ericsson M, Mincheva-Nilsson L, et al. Microvesicle-associated AAV vector as a novel gene delivery system. Mol Ther. 2012; 20(5):960–971. [PubMed: 22314290]
14. Alvarez-Erviti L, Seow Y, Yin H, Betts C, Lakhal S, Wood MJ. Delivery of siRNA to the mouse brain by systemic injection of targeted exosomes. Nat Biotechnol. 2011; 29(4):341–345. [PubMed: 21423189]
15. Sun D, Zhuang X, Xiang X, Liu Y, Zhang S, Liu C, et al. A novel nanoparticle drug delivery system: the anti-inflammatory activity of curcumin is enhanced when encapsulated in exosomes. Mol Ther. 2010; 18(9):1606–1614. [PubMed: 20571541]
16. Ohno S, Takanashi M, Sudo K, Ueda S, Ishikawa A, Matsuyama N, et al. Systemically injected exosomes targeted to EGFR deliver antitumor microRNA to breast cancer cells. Mol Ther. 2013; 21(1):185–191. [PubMed: 23032975]
17. Dai S, Wei D, Wu Z, Zhou X, Wei X, Huang H, et al. Phase I clinical trial of autologous ascites-derived exosomes combined with GM-CSF for colorectal cancer. Mol Ther. 2008; 16(4):782–790. [PubMed: 18362931]
18. Maguire CA, Crommentuijn MH, Mu D, Hudry E, Serrano-Pozo A, Hyman BT, et al. Mouse gender influences brain transduction by intravascularly administered AAV9. Mol Ther. 2013; 21(8):1470–1471. [PubMed: 23903572]
19. Atai NA, Balaj L, van Veen H, Breakefield XO, Jarzyna PA, Van Noorden CJ, et al. Heparin blocks transfer of extracellular vesicles between donor and recipient cells. J Neurooncol. 2013; 115(3):343–351. [PubMed: 24002181]
20. Christianson HC, Svensson KJ, van Kuppevelt TH, Li JP, Belting M. Cancer cell exosomes depend on cell-surface heparan sulfate proteoglycans for their internalization and functional activity.2013. Proc Natl Acad Sci U S A. 110(43):17380–17385. [PubMed: 24101524]
21. Bell CL, Vandenberghe LH, Bell P, Limberis MP, Gao GP, Van Vliet K, et al. The AAV9 receptor and its modification to improve in vivo lung gene transfer in mice. J Clin Invest. 2011; 121(6): 2427–2435. [PubMed: 21576824]
22. Gyorgy B, Modos K, Pallinger E, Paloczi K, Pasztoi M, Misjak P, et al. Detection and isolation of cell-derived microparticles are compromised by protein complexes resulting from shared biophysical parameters. Blood. 2011; 117(4):e39–e48. [PubMed: 21041717]
23. Kumar P, Wu H, McBride JL, Jung KE, Kim MH, Davidson BL, et al. Transvascular delivery of small interfering RNA to the central nervous system. Nature. 2007; 448(7149):39–43. [PubMed: 17572664]
24. Tannous BA, Grimm J, Perry KF, Chen JW, Weissleder R, Breakefield XO. Metabolic biotinylation of cell surface receptors for in vivo imaging. Nat Methods. 2006; 3(5):391–396. [PubMed: 16628210]

25. Gao Q, Liu YJ, Guan ZZ. Oxidative stress might be a mechanism connected with the decreased alpha 7 nicotinic receptor influenced by high-concentration of fluoride in SH-SY5Y neuroblastoma cells. Toxicol In Vitro. 2008; 22(4):837–843. [PubMed: 18282683]
26. Murphy SL, Li H, Zhou S, Schlachterman A, High KA. Prolonged susceptibility to antibody-mediated neutralization for adeno-associated vectors targeted to the liver. Mol Ther. 2008; 16(1): 138–145. [PubMed: 17955024]
27. Jiang H, Couto LB, Patarroyo-White S, Liu T, Nagy D, Vargas JA, et al. Effects of transient immunosuppression on adeno-associated, virus-mediated, liver-directed gene transfer in rhesus macaques and implications for human gene therapy. Blood. 2006; 108(10):3321–3328. [PubMed: 16868252]
28. Manno CS, Pierce GF, Arruda VR, Glader B, Ragni M, Rasko JJ, et al. Successful transduction of liver in hemophilia by AAV-Factor IX and limitations imposed by the host immune response. Nat Med. 2006; 12(3):342–347. [PubMed: 16474400]
29. Lin J, Calcedo R, Vandenberghe LH, Figueredo JM, Wilson JM. Impact of preexisting vector immunity on the efficacy of adeno-associated virus-based HIV-1 Gag vaccines. Hum Gene Ther. 2008; 19(7):663–669. [PubMed: 18549307]
30. Bar S, Daeffler L, Rommelaere J, Nuesch JP. Vesicular egress of non-enveloped lytic parvoviruses depends on gelsolin functioning. PLoS Pathog. 2008; 4(8):e1000126. [PubMed: 18704167]
31. Bhattacharya B, Roy P. Role of lipids on entry and exit of bluetongue virus, a complex non-enveloped virus. Viruses. 2010; 2(5):1218–1235. [PubMed: 21994677]
32. Doria M, Ferrara A, Auricchio A. AAV2/8 vectors purified from culture medium with a simple and rapid protocol transduce murine liver, muscle, and retina efficiently. Hum Gene Ther Methods. 2013; 24(6):392–398. [PubMed: 24116943]
33. Manning WC, Zhou S, Bland MP, Escobedo JA, Dwarki V. Transient immunosuppression allows transgene expression following readministration of adeno-associated viral vectors. Hum Gene Ther. 1998; 9(4):477–485. [PubMed: 9525309]
34. Mingozzi F, Anguela XM, Pavani G, Chen Y, Davidson RJ, Hui DJ, et al. Overcoming preexisting humoral immunity to AAV using capsid decoys. Sci Transl Med. 2013; 5(194):194ra92.
35. Chicoine L, Montgomery C, Bremer W, Shontz K, Griffin D, Heller K, et al. Plasmapheresis eliminates the negative impact of AAV antibodies on microdystrophin gene expression following vascular delivery. Mol Ther. 2014; 22(2):338–347. [PubMed: 24196577]
36. Mimuro J, Mizukami H, Hishikawa S, Ikemoto T, Ishiwata A, Sakata A, et al. Minimizing the inhibitory effect of neutralizing antibody for efficient gene expression in the liver with adeno-associated virus 8 vectors. Mol Ther. 2013; 21(2):318–323. [PubMed: 23247100]
37. Maheshri N, Koerber JT, Kaspar BK, Schaffer DV. Directed evolution of adeno-associated virus yields enhanced gene delivery vectors. Nat Biotechnol. 2006; 24(2):198–204. [PubMed: 16429148]
38. Foust KD, Nurre E, Montgomery CL, Hernandez A, Chan CM, Kaspar BK. Intravascular AAV9 preferentially targets neonatal neurons and adult astrocytes. Nat Biotechnol. 2009; 27(1):59–65. [PubMed: 19098898]
39. Sallach J, Di Pasquale G, Larcher F, Niehoff N, Rubsam M, Huber A, et al. Tropism-modified AAV vectors overcome barriers to successful cutaneous therapy. Mol Ther. 2014; 22(5):929–939. [PubMed: 24468915]
40. Gray SJ, Blake BL, Criswell HE, Nicolson SC, Samulski RJ, McCown TJ, et al. Directed evolution of a novel adeno-associated virus (AAV) vector that crosses the seizure-compromised blood-brain barrier (BBB). Mol Ther. 2010; 18(3):570–578. [PubMed: 20040913]
41. Grimm D, Lee JS, Wang L, Desai T, Akache B, Storm TA, et al. In vitro and in vivo gene therapy vector evolution via multispecies interbreeding and retargeting of adeno-associated viruses. J Virol. 2008; 82(12):5887–5911. [PubMed: 18400866]
42. Kim SS, Ye C, Kumar P, Chiu I, Subramanya S, Wu H, et al. Targeted delivery of siRNA to macrophages for anti-inflammatory treatment. Mol Ther. 2010; 18(5):993–1001. [PubMed: 20216529]

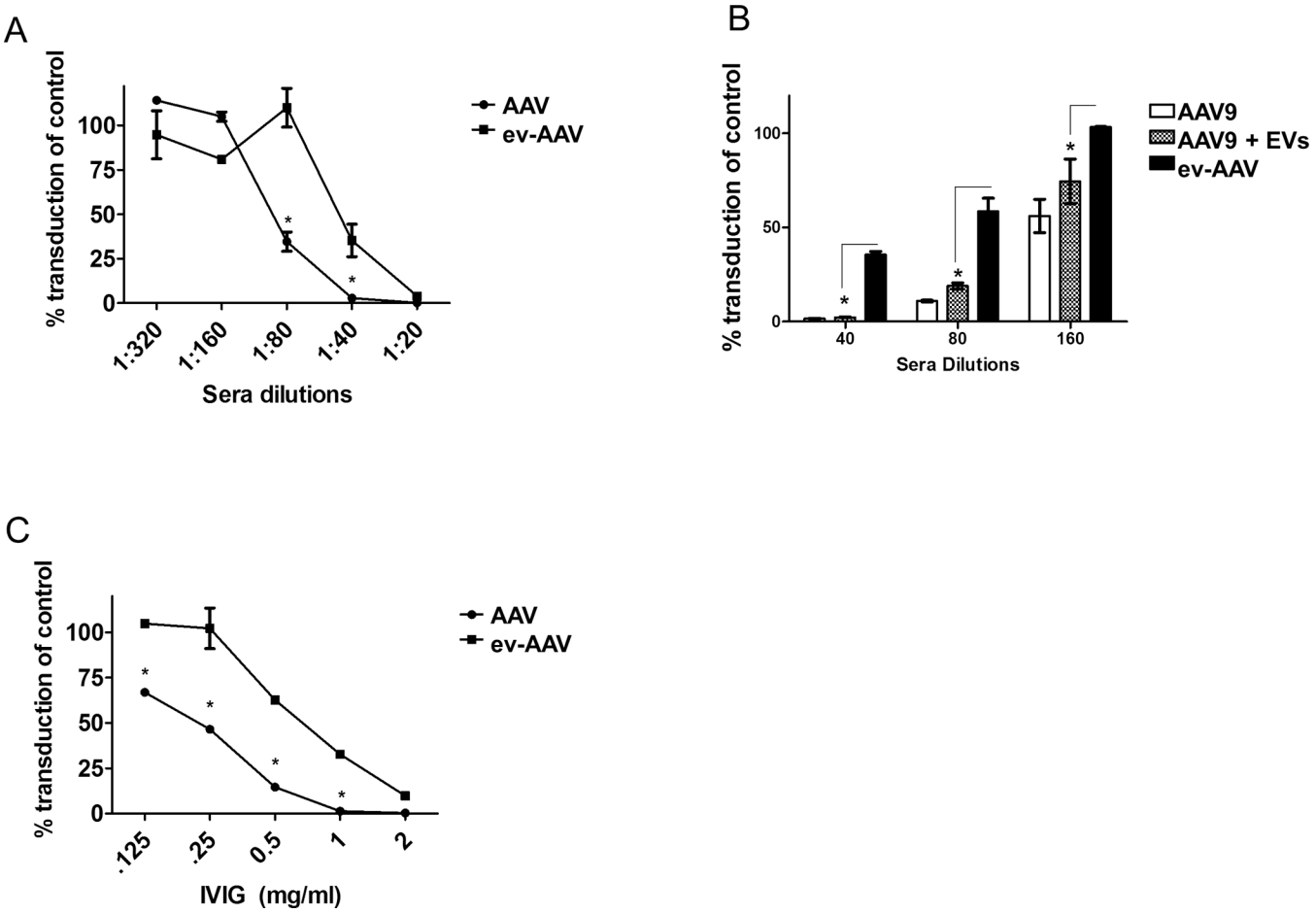

Figure 1. ev-AAV evade neutralizing antibodies from pooled human serum and purified pooled human intravenous immunoglobulin (IVIg)

(A) Dilutions of pooled human sera (10 donors) were mixed with either standard AAV9-FLuc or ev-AAV9-FLuc. After incubation for 1 h, mixtures were added to HeLa cells and two days later an FLuc assay was performed. FLuc levels were normalized to the levels achieved in the absence of serum. **(B)** Mixing EVs with standard AAV does not result in significantly enhanced protection from pooled human serum observed with ev-AAV. Standard AAV9-FLuc, AAV9-FLuc mixed with extracellular vesicles, or ev-AAV9-FLuc were mixed with the indicated dilutions of pooled human serum. A neutralization assay was performed on as in (A). **(C)** Dilutions of IVIg were made and a neutralization assay performed as in (A). *$p<0.05$.

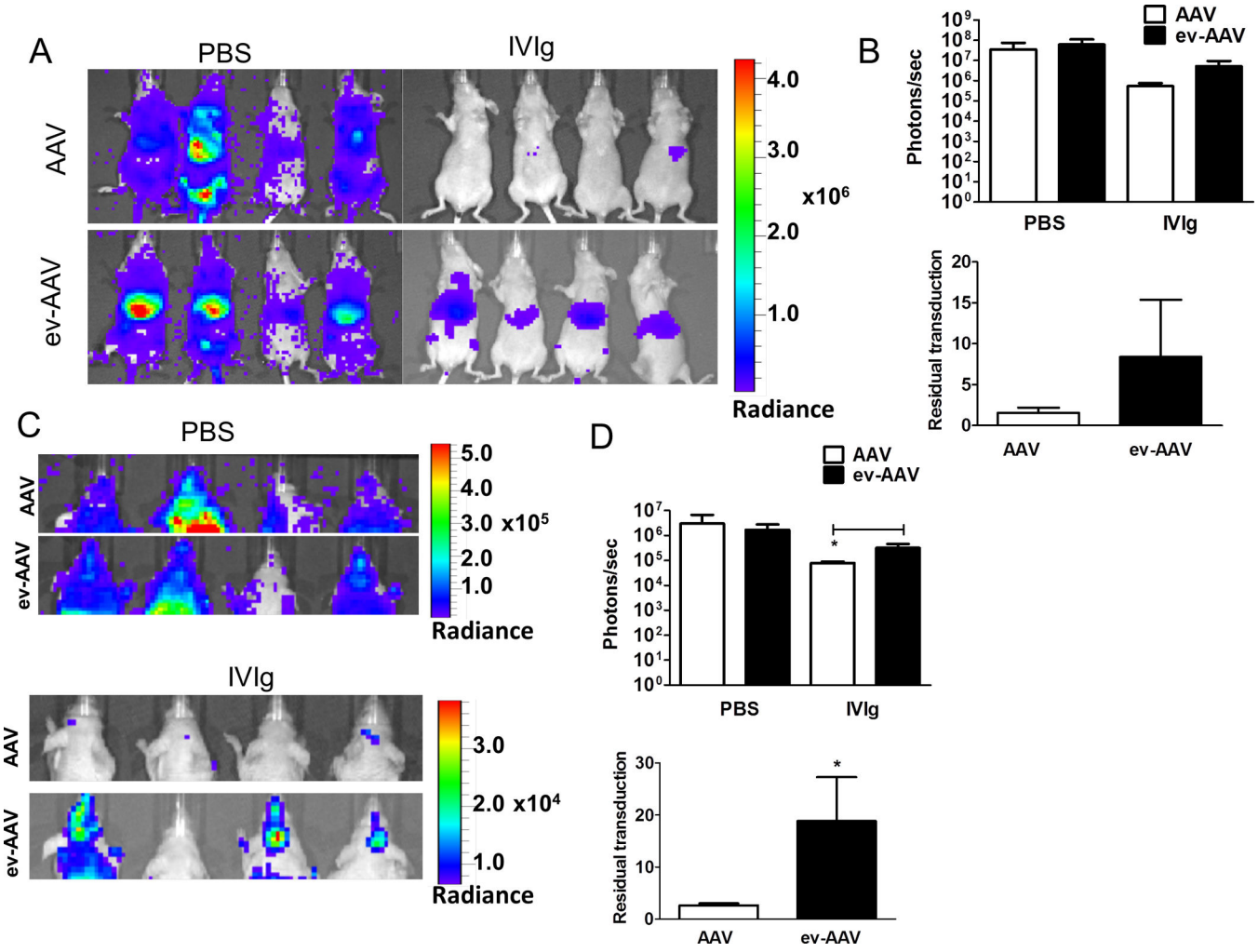

Figure 2. ev-AAV evades neutralizing anti-AAV antibodies more efficiently than AAV *in vivo*

Mice were injected with PBS or 0.5 mg IVIg/mouse and 24 h later challenged with 10^{10} g.c. of either standard AAV9-FLuc or ev-AAV9-FLuc. Seven days later mice were imaged for FLuc expression by bioluminescent imaging. **(A)** Bioluminescence images of animals in ventral view. **(B)** Top, photon flux in liver region for each group after PBS pre-treatment or, IVIg pre-treatment; bottom, calculation of residual transduction in liver region of AAV or ev-AAV in the presence of IVIg when compared to transduction after i.p. injection of PBS. n=4, p=0.099. **(C)** Top, bioluminescence images of all groups of animals in dorsal view. Bottom, IVIG groups shown with lowered scale to clearly indicate higher residual FLuc signal in the head of ev-AAV injected mice. **(D)** Top, photon flux in head region for each group after PBS pre-treatment or IVIg pre-treatment; bottom, calculation of residual transduction in head region of AAV or ev-AAV in the presence of IVIg when compared to transduction after i.p. injection of PBS. *p=0.0085. Radiance= photons/sec/cm^2/sr.

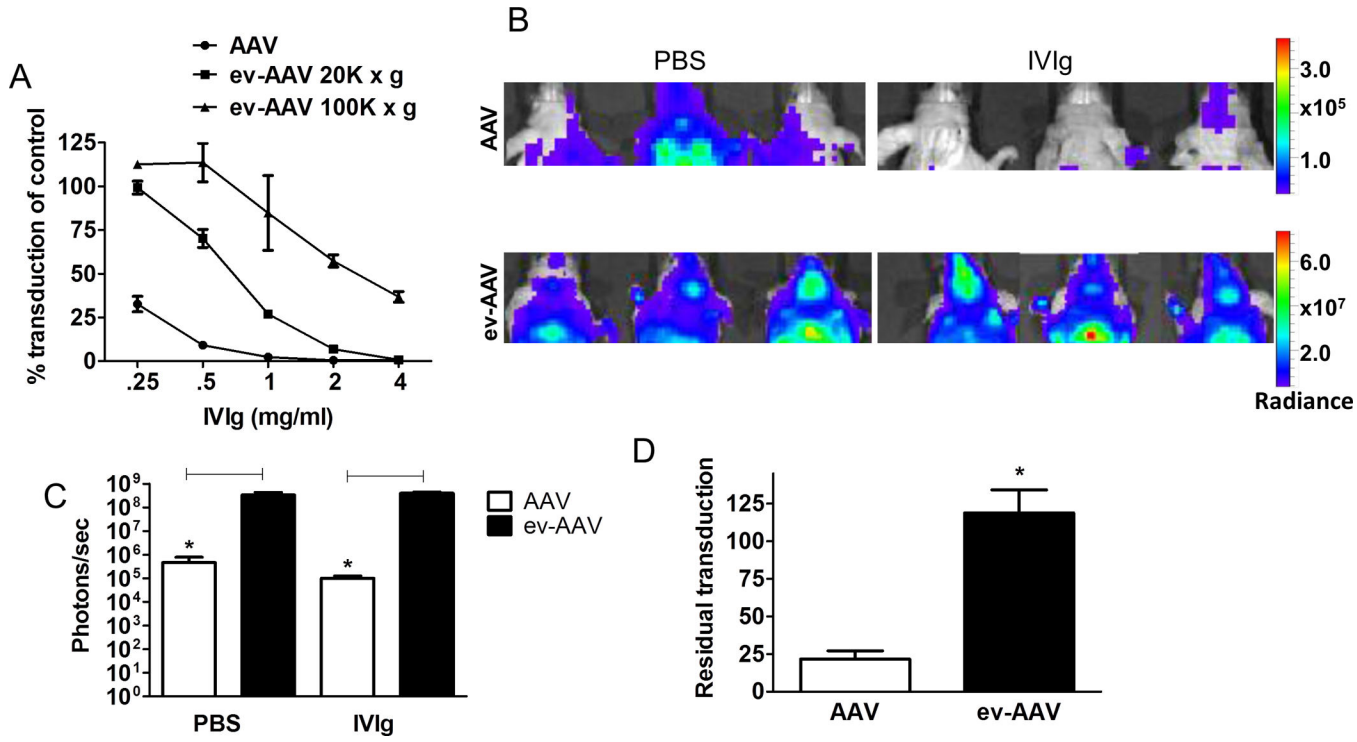

Figure 3. 100k × g ev-AAV9 fraction has enhanced antibody evasion properties

(A) A neutralization assay identical to Fig. 1C with IVIg, using AAV9, 20k × g ev-AAV9, 100k × g ev-AAV9. **(B)** Mice were injected with PBS or 0.5 mg IVIg/mouse and 24 h later challenged with 10^{10} g.c. of either standard AAV9-FLuc or 100k × g ev-AAV9-FLuc. Fourteen days later mice were imaged for FLuc expression by bioluminescent imaging. Bioluminescent images of the head region are shown. Note the scale differences between standard AAV and ev-AAV groups. **(C)** Photon flux of head region for standard AAV9-FLuc or 100k × g ev-AAV9-FLuc with PBS or IVIg pretreatment. **(D)** Residual transduction in the IVIg groups relative to PBS pretreatment groups. *, $p<0.05$.

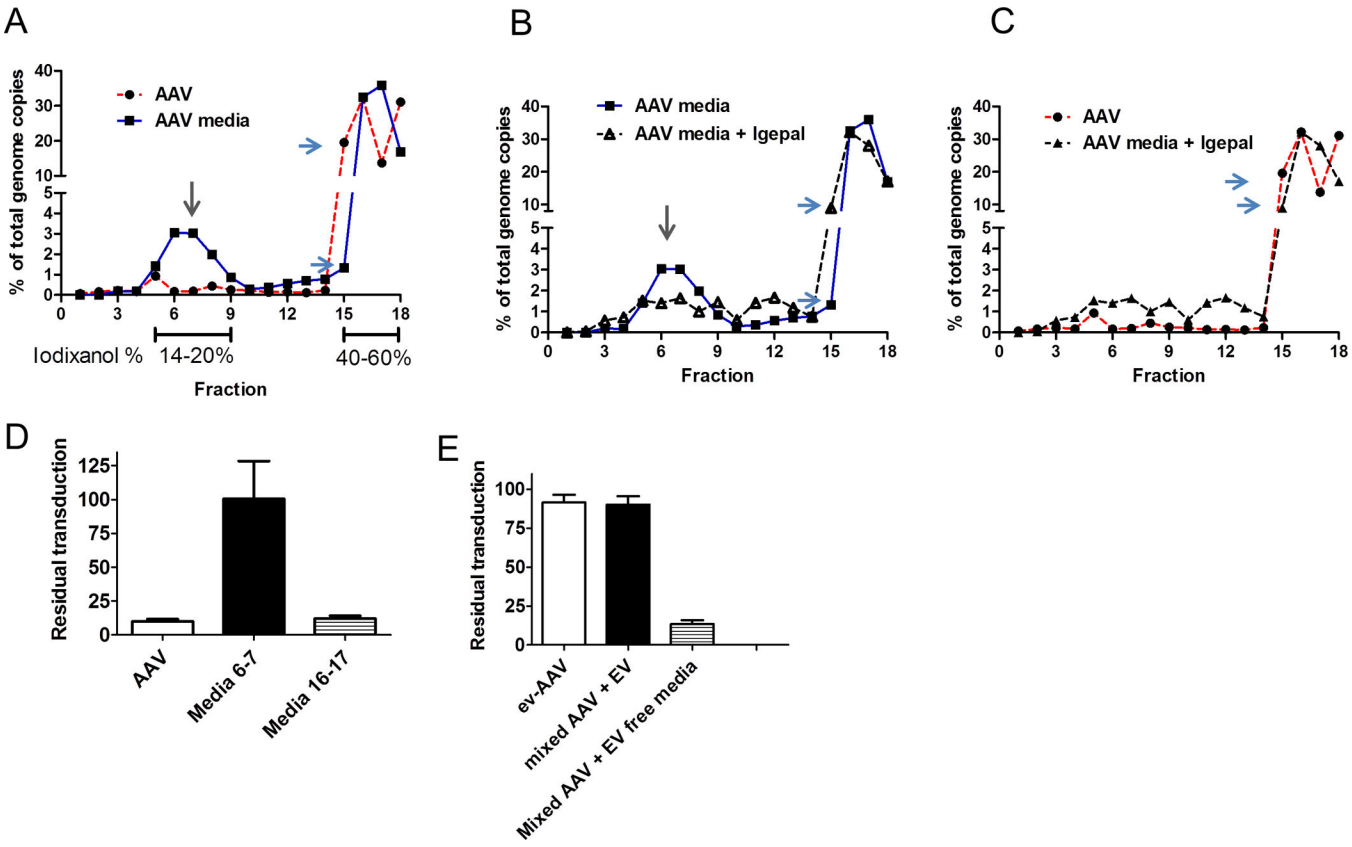

Figure 4. 20k × g depleted media (used for 100k × g ev-AAV isolation) contains an antibody resistant fraction

(A) A AV genome distribution in fractions of a 8–60% iodixanol gradient loaded with standard AAV (red line) or 20k × g depleted media from AAV9 producing-293T cells (blue line**)**. The putative vesicle-associated fractions of AAV is indicated by a gray arrow. Differences in the amount in fraction #15 between the two samples is indicated by blue arrows. **(B)** Treatment with Igepal detergent (black line) partially disrupts vesicle fraction. Untreated AAV in media is indicated by blue line. **(C)** Comparison of Igepal treated media sample with standard free AAV. **(D)** Antibody resistance (IVIG) profile of free standard AAV, or AAV in media fractions 6–7 or 16–17 from (A) **(E)** Mixing free AAV with EV containing media and centrifuging at 100k × g results in antibody resistant vector. Removing EVs from the same media restores sensitivity to antibody neutralization.

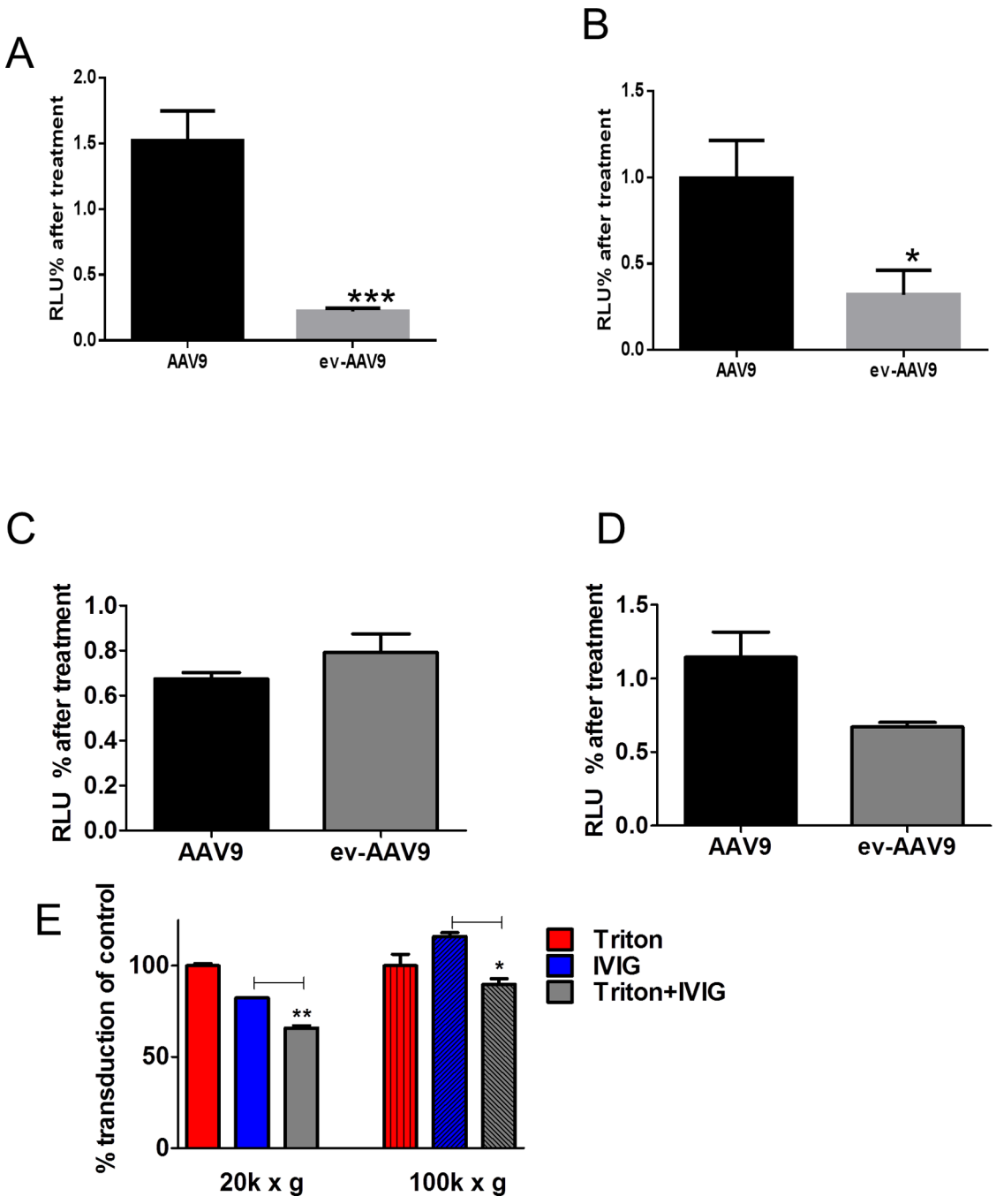

Figure 5. Transduction properties of AAV9 20k × g ev-AAV9 and 100k × g ev-AAV9 fractions

(A) Heparin blocks 20k × g ev-AAV9 transduction. AAV9-FLuc and ev-AAV9-FLuc were incubated with 50 μg/ml heparin and then added to cells. Fluc activity was measured 48 h later and normalized to transduction in the absence of heparin. **(B)** Triton treatment of 20k × g ev-AAV9 reduces transduction efficiency. AAV9-FLuc and ev-AAV9-FLuc were incubated with 0.3% Triton before diluting and adding to cells. Transduction was normalized to luciferase activity in the absence of Triton. **(C)** Even higher concentrations of heparin (100 ug/ml) did not inhibit 100k × g ev-AAV9 more than AAV9. **(D)** Triton

treatment had a modest effect on 100k × g ev-AAV9 transduction. **(E)** Triton treatment breaks open EVs and reduces resistance to antibodies in 20k × g and 100k × g fractions. *** $p<0.001$,**$p<0.006$, *$p<0.05$.

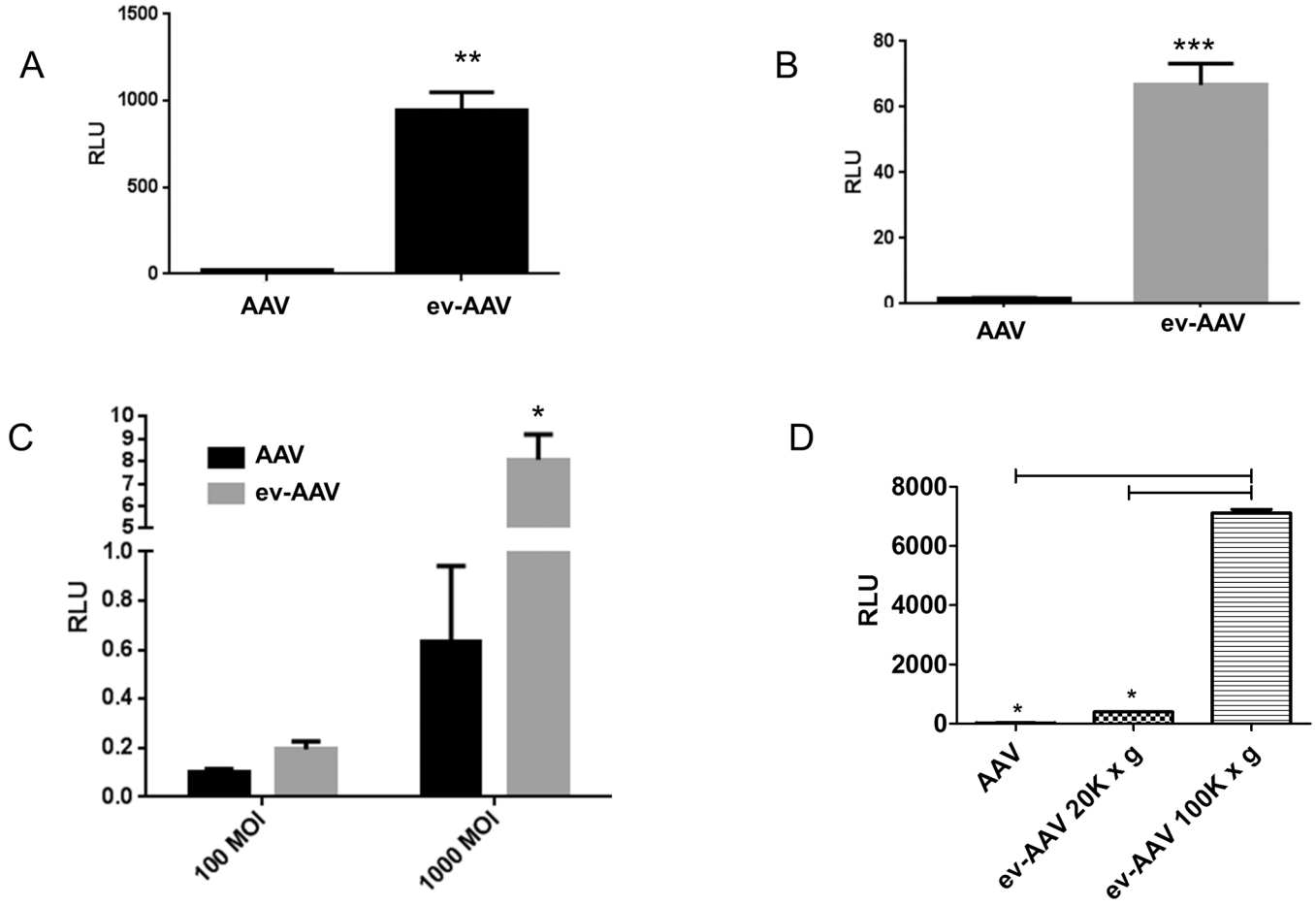

Figure 6. ev-AAV9-FLuc is more efficient in culture at transduction than standard AAV9-FLuc

(A) primary murine neurons (B) SH-SY5Y cells (C) melanocytes. Cells were incubated with AAV9-FLuc or ev-AAV9-FLuc and 48 h later an luciferase assay performed. (D) Comparison of AAV9, and 20k × g and 100k × g fractions of ev-AAV at transduction of HeLa cells. **p=0.006; ***p<0.0001 *; p= 0.012. RLU= Relative light units

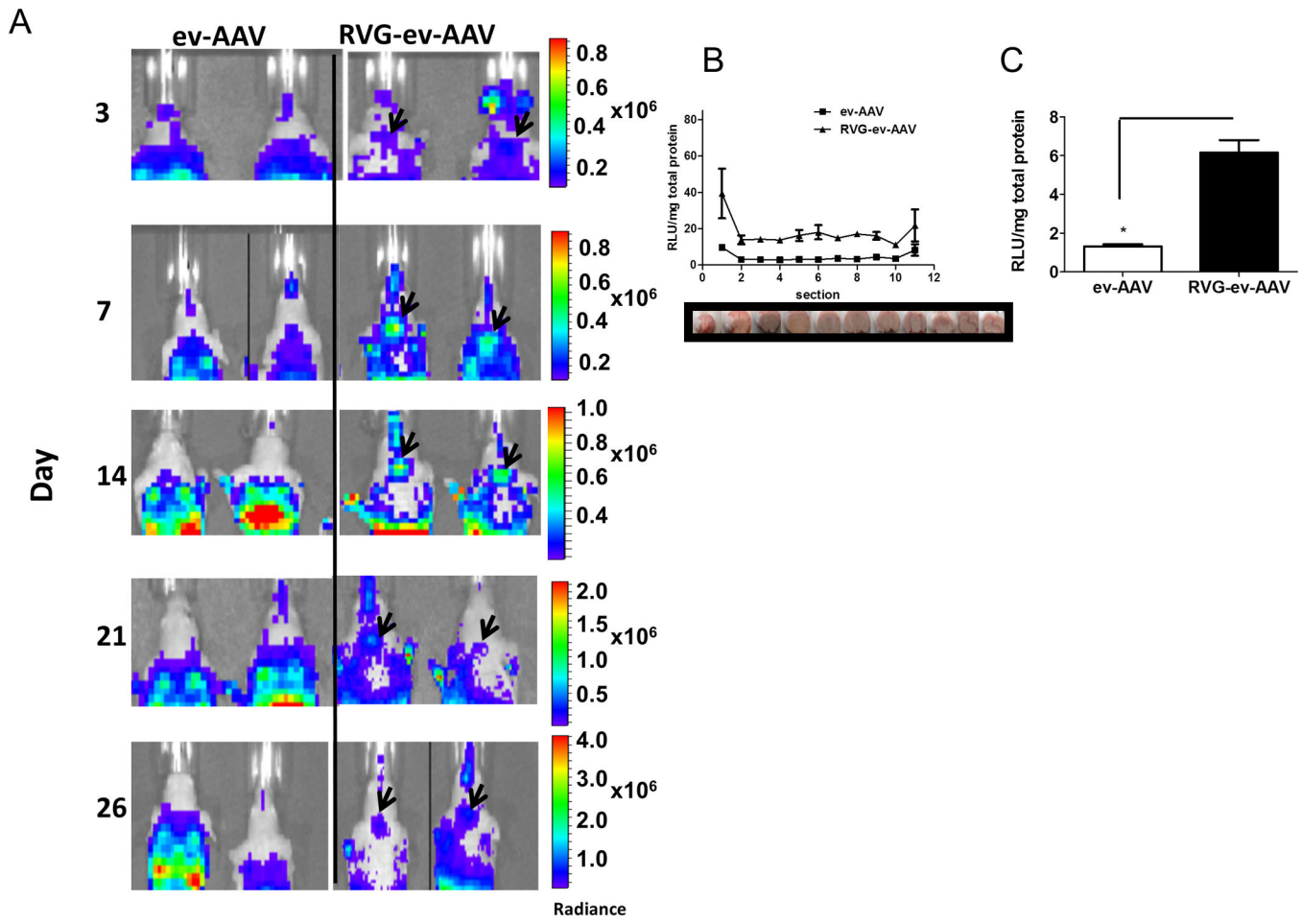

Figure 7. RVG-ev-AAV9-FLuc enhances brain transduction compared to untargeted ev-AAV9-Fluc

(A) Bioluminescent images of head region in mice in ev-AAV9-FLuc and RVG-ev-AAV9-FLuc groups. Note the circular pattern of bioluminescence eminating from the brain of RVG-ev-AAV9-FLuc mice (black arrowheads) which indicate this vector is transducing brain better than ev-AAV9-FLuc. **(B)** Day 32 post-injection mice were sacrificed and brains cryosectioned coronally in 1 mm sections. Each section was homogenized and luciferase activity as well as total protein content determined to give a Fluc expression profile for the entire brain for each group of mice. The brain images below the graph show the approximate location of the section taken for measurement. **(C)** Average RLU/mg in striatum sections for all three groups. n=4;*, $p<0.05$. Radiance= photons/sec/cm^2/sr. RLU= Relative Light Unit.

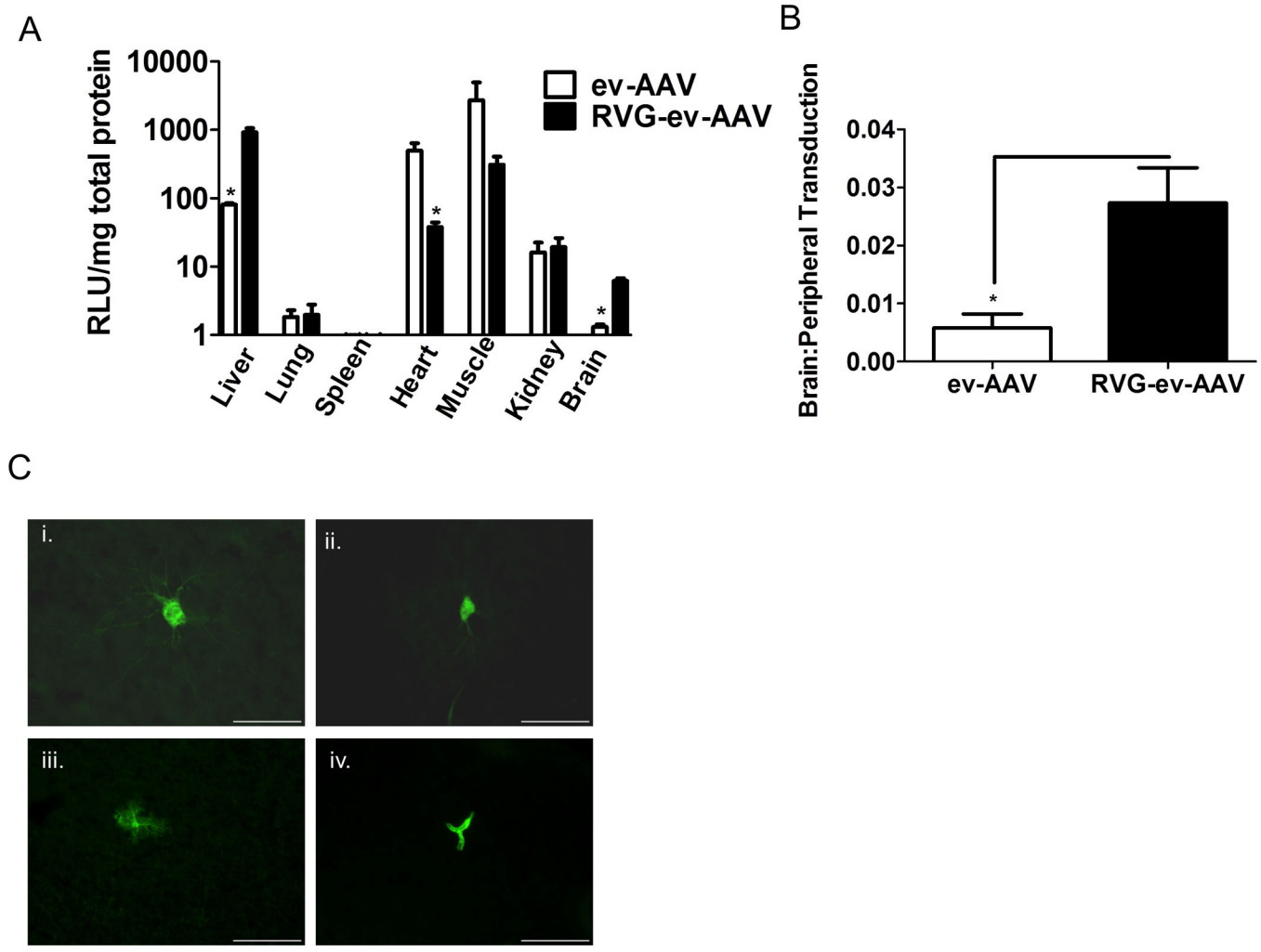

Figure 8. RVG-ev-AAV9-FLuc enhances transduction specificity for the brain after i.v. injection

(A) FLuc activity in tissue homogenates. n=4; *=p<0.05. **(B)** brain targeting specificity calculated from the ratio of brain transduction to peripheral organ transduction. *, p<0.05. **(C)** RVG-ev-AAV9-GFP transduced cell types in the brain. Vector was injected i.v. and two weeks later fixed sections were immunostained for GFP. GFP positive neurons (i, ii.), astrocytes (iii.), and endothelial cells (iv.) were observed. Scale bar= 55 μm. RLU= Relative Light Unit.

Table I

Percent of total AAV in media in EV fractions

Sample	20k × g EV pellet	100k × g EV pellet
ev-AAV9*	0.99 +/− 0.11%	40.1 +/− 3.21%
Standard AAV9 + EV mix#	0.087 +/− 0.009%	38.3 +/− 4.24%

*Media harvested from 293T cells transfected with AAV9-Fluc plasmids

#Media harvested from *non-transfected* 293T. Standard, iodixanol purified AAV was spiked into the EV-containing media and then the samples were centrifuged at either 20,000 × g or 100,000 × g and AAV genomes in the EV pellet determined by qPCR.